Cycle and performance analysis of a small-scale adsorption heat transformer for desalination and cooling applications

Cycle and performance analysis of a small-scale adsorption heat transformer for desalination and cooling applications

C. Olkis[a], S. Brandani[a] and G. Santori[a]*

[a] *The University of Edinburgh, School of Engineering, Institute for Materials and Processes, Sanderson Building, The King's Buildings, Mayfield Road, EH9 3FB Edinburgh, Scotland, UK*

*Corresponding author: G.Santori@ed.ac.uk

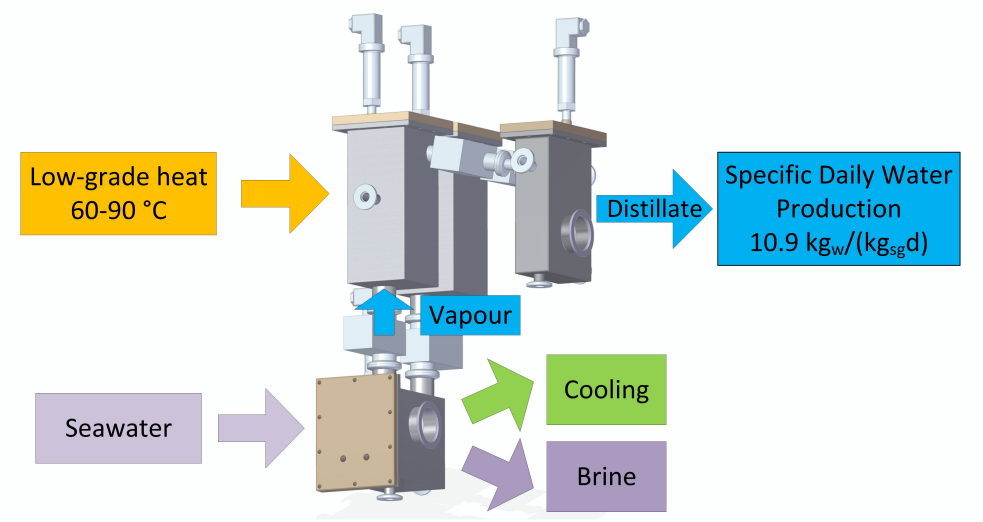

Abstract

Adsorption heat transformers use low-grade heat to produce potable water and provide cooling at the same time. In this study, we present a comprehensive performance analysis for an experimental system featuring the world's smallest design using silica gel, which is commonly used as benchmarking material. We analyse the system performance in a thorough cycle analysis that quantifies the influence of isosteric heating times and cycle times onto the adsorption working capacity. In addition, the performance is assessed through common performance indicators for desalination as well as cooling. We found that the system achieved a Specific Daily Water Production of up to 10.9 $kg_w/(kg_{sg}d)$ at 80 °C. The combination of cooling and desalination is discussed highlighting advantages as well as disadvantages, which are often neglected. The results show that silica gel has a high performance in desalination, which decreases by more than 60 % if cooling is desired as well.

Keywords: Desalination, Refrigeration, Adsorption, Silica Gel, Adsorption Cycle

1. Introduction

Two billion people will be affected by water scarcity by 2025 and the demand for water is estimated to rise by 40 % until 2050 [1, 2]. Desalination offers a solution to face this challenge and to supplement the natural freshwater resources. Most-commonly, seawater is desalinated using reverse osmosis membranes, which consume large quantities of electricity and are troubled by membrane fouling [3]. By contrast, thermal desalination techniques need less electric energy, because they are essentially driven by low-grade heat sources. Moreover, thermal desalination [4, 5] can be linked up with Reverse Electrodialysis membranes to generate electricity from low-grade heat [6, 7]. The two most common commercial thermal desalination systems [8] are multi-stage flash [9] and multi-effect distillation [10] operating at top brine temperatures of 90 °C and 70 °C respectively [11]. Membrane distillation is another commercial technology suitable for smaller applications, which is usually driven by low-grade heat 60-90 °C [12, 13]. However, no technologies can efficiently utilise low-grade heat below 50 °C despite the vast availability of heat at very low temperatures [14]. Adsorption desalination is a novel thermally driven method that can utilise heat as low as 50 °C [15] with the potential to fill the ultra-low temperature niche. Most systems apply silica gel-water as working pair in desalination [15–17] as well as refrigeration [18–20].

A key aspect of research carried out on adsorption desalination and refrigeration is the performance assessment [21, 22], which is usually focused on the performance indicators examining the energy efficiency and the daily water production [15]. Several adsorption desalinators combined with cooling have been built achieving a maximum specific daily water production of 1.8 $kg_w/(kg_{sg}d)$ [16], 4.0 $kg_w/(kg_{sg}d)$ [17] and 14.2 $kg_w/(kg_{sg}d)$ [15] all at 85 °C. However, the study of Ng et al. showed that the specific daily water production is strongly temperature dependent and is reduced from 14.2 to 4.2 $kg_w/(kg_{sg}d)$ for a heat source temperature of 60 °C, but experiments have shown the feasibility of the process at 50 °C [15]. Pan et al. presented a high performing experimental adsorption chiller using silica gel-water [23]. They reported a Coefficient of Performance of 0.51 and Specific Cooling Capacity of 125 W/kg_{sg} providing cooling at 11 °C at a heat source of 86 °C [23].

The system analysis through performance indicators alone does not give an indication of the factors leading to an improvement of the process. Conversely, the analysis of the adsorption cycle enables the experimental evaluation of the actual working capacity or cycle time. Previous investigations have studied the influence of the overall heat transfer coefficient of the heat

exchangers on the adsorption cycle [24]. Douss et al. demonstrated that an undersized evaporator or condenser heat exchanger changes the shape of the adsorption cycle significantly [24]. Chua et al. presented the adsorption cycle for insufficient isosteric heating times in a dynamic, lumped-parameter simulation [25]. In a theoretical study, Wu et al. assessed the performance of adsorption desalinators through an analysis of the thermodynamic adsorption cycle focusing on different temperature levels [26].

A detailed experimental study of the adsorption cycle to present a novel system design has not been performed yet. In addition, there remains a need for critical performance analysis for silica gel on desalination combined with cooling as publications usually do not highlight the disadvantages.

This work presents results obtained for silica gel using a novel, small-scale adsorption desalinator, where the size of the adsorption beds is reduced by more than two orders of magnitude compared to other systems [27]. The experimental adsorption cycle was assessed for different cycle times along with a comparison to the thermodynamic adsorption cycle. The analysis quantifies how the change of process parameters alters the deviation of the experimental adsorption cycle from the ideal case. Furthermore, the system's performance is studied in terms of the Specific Daily Water Production and specific cooling capacity in comparison to the best performing adsorption desalinator in the literature. The performance indicators are analysed for different temperature combinations and cycle times. The system is also critically analysed for the combined output of potable water and cooling. The results of the combined process using silica gel are compared to other adsorption materials presented in the literature.

2. The adsorption process and cycle

In the basic set-up a temperature swing adsorption desalination systems consists of an evaporator, two adsorber vessels and a condenser [28] as given in the process flow diagram (Fig. 1a) and in the photograph of the experimental set-up (Fig. 1b), which is described in detail elsewhere [29]. Each one of the vessels features a heat exchanger and each heat exchanger is connected to one of three thermostatic baths supplying cooling or heating water to power the process and maintain temperatures inside the vessels (Fig. 1a).

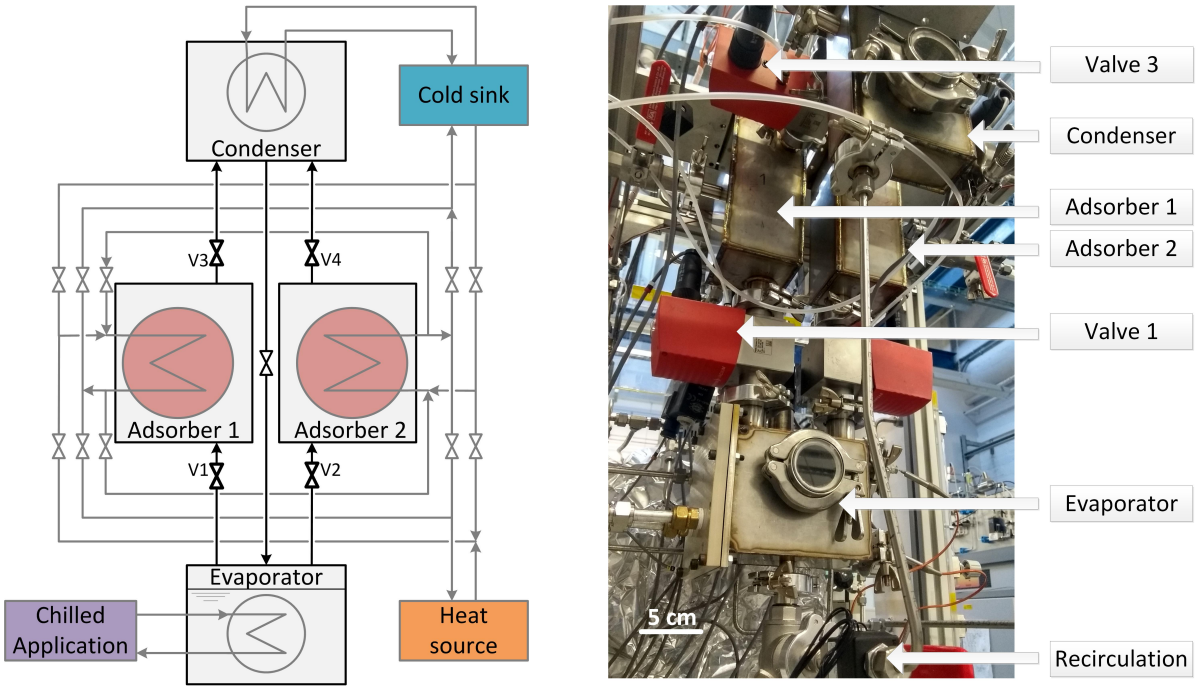

Figure 1: (a) Process flow diagram of the adsorption test rig with the four vessels as main components and the heating/cooling water supply loops connected to three thermostatic baths. The inner heating/cooling water loop represents the heat recovery between the two adsorber beds.
(b) Photgraph of the small-scale test rig with its four vacuum vessels, four vacuum valves and the recirculation line.

Each adsorber bed undergoes a cycle of pressure and temperature changes as displayed by the temperature curves in Fig. 2a and the corresponding thermodynamic cycle of Fig. 2b. The thermodynamic cycle represents the equilibrium states and is time independent, whereas the experimental cycle is determined by the cycle times and heat/mass transfer limitations.

At point 1 (Fig. 2a and 2b), the adsorption material is in equilibrium with water vapour, both valves V1 and V3 are closed, and the pressures of the evaporator and adsorber are equal. In this step the bed is heated to increase the bed pressure to the condenser pressure (isosteric heating). The bed moves from point 1 to point 2 with negligible desorption occurring. The material can be assumed to remain on the same isostere q_{high}. Once the adsorber is at the same pressure as the condenser, valve V3 is opened and water starts to desorb, while the bed is heated.

The total heat energy input into the system includes the heat required to bring the heat exchangers and adsorption material from ambient to regeneration temperature and the heat of desorption. When the bed has reached point 3, where the bed temperature equals the heat source temperature, valve V3 is closed again. The bed is then cooled to decrease the pressure back to the evaporator pressure. The isosteric cooling happens along the lean isostere of the material q_{low}. As soon as the bed and the evaporator pressures are equal, valve V1 is opened to

connect the bed to the evaporator to start water vapour adsorption. The bed is cooled until it reaches ambient temperature.

The working capacity Δq [kg_w/kg_{sg}] of the cycle is determined by the distance between the two isosteres q_{high} and q_{low}. It is an important property in adsorption desalination, because it determines the amount of water produced per cycle. The working capacity can be maximised by operating the condenser and evaporator at equal pressures $P_{cond} = P_{evap}$. In this case point 1 moves up to point 5 in Fig. 2b altering the cycle to only one straight line 5→3 for desorption and 5←3 for adsorption. In theory, this case does not require isosteric heating as the entire system operates at only one pressure level. However, maintaining the system at one pressure level is challenging, because the cooling effect of the evaporating water decreases the evaporator pressure.

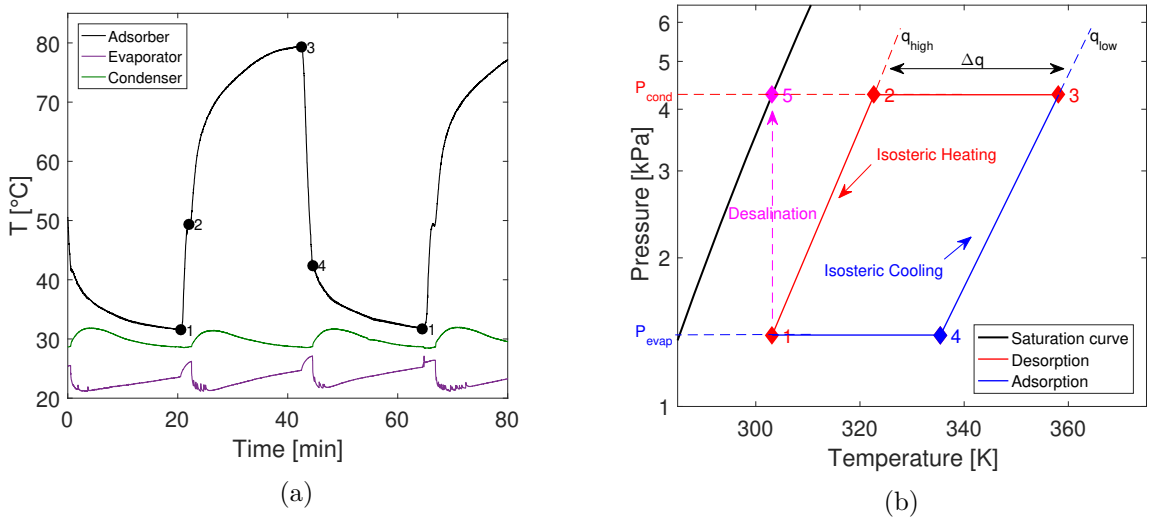

Figure 2: (a) Experimental temperature curves corresponding to the heating and cooling phases of the adsorption material in (b).
(b) An exemplary thermodynamic adsorption cycle including the working capacity q_{high}-q_{low}=Δq

3. Performance indicators

The main performance indicators for adsorption desalination are the Performance Ratio PR [-] and Specific Daily Water Production $SDWP$ [$kg_w/(kg_w d)$]:

$$PR = \int_0^{t_{cycle}} \frac{\dot{m}_{water} \cdot L_w}{\dot{Q}_{des}} dt \tag{1}$$

$$SDWP = N \int_0^{t_{cycle}} \frac{\dot{Q}_{cond}}{L \cdot M_{sg}} dt \tag{2}$$

Adsorption chilling is characterised by the Coefficient of Performance COP [-] and the specific cooling capacity SCC [W/kg_{sg}]:

$$COP = \int_0^{t_{cycle}} \frac{\dot{Q}_{evap}}{\dot{Q}_{des}} dt \tag{3}$$

$$SCC = \int_0^{t_{cycle}} \frac{\dot{Q}_{evap}}{M_{sg}} dt \tag{4}$$

where N [-] is the number of cycles per day, which is defined by N = $86400\frac{s}{d}$ / t_{cycle}. T_{cyle} is the cycle time [s], $M_{\mathrm{sg}} = 0.4$ kg is the total mass of silica gel and L_{w} is the latent heat of water. A standardised latent heat of water $L_{\mathrm{w}} = 2326$ kJ/kg_{w} was used to make the results more comparable as introduced in different other publications The water uptake per cycle increases with the cycle time, but longer cycle times reduce the number of cycles per day N
The energy balances to determine the heat input to each vessel [kJ/s] are:

$$\dot{Q}_{des} = \dot{m}_{hot}\ c_{p,w}\ (T_{des,in} - T_{des,out}) \tag{5}$$

$$\dot{Q}_{evap} = \dot{m}_{evap}\ c_{p,w}\ (T_{evap,in} - T_{evap,out}) \tag{6}$$

$$\dot{Q}_{cond} = \dot{m}_{cond}\ c_{p,w}\ (T_{cond,in} - T_{cond,out}) \tag{7}$$

Where ṁ is the mass flow rate of water from the thermostatic bath [kg/s], $c_{\mathrm{p,w}}$ is the specific heat of water [kJ/(kgK)] and the temperature difference between the inlet T_{in} and outlet T_{out} to the heat exchanger [K].

The SDWP can also be estimated theoretically by assessing the working capacity of the adsorption material Δq through its isotherm. The Dubinin Astakhov (DA) isotherm depicts the water silica gel system well [30]. DA determines the equilibrium uptake q [$kg_{\mathrm{w}}/kg_{\mathrm{sg}}$] of the material at points 1 and 3 of the thermodynamic cycle in Fig. 2b by $\Delta q = q_1 - q_3$. The DA-isotherm is defined as [31, 32]:

$$q_i = q_0\ exp\left[-\left(\frac{A}{E}\right)^n\right] \tag{8}$$

$$A = -RT\ ln\left(\frac{P}{P_{sat}}\right) \tag{9}$$

Where q_0 [kg/kg], E [kJ/kg] and n [-] are the Dubinin Astakhov parameters given among other experimental parameters in table 1.

Table 1: Parameter table for Siogel silica gel experiments.

Parameter	**Unit**	**Value**	**Ref.**
q_0	(kg_w/kg_{sg})	0.38	[30]
E	(kJ/kg)	220	[30]
n	(-)	1.1	[30]
M_{sg}	(kg)	ea. 0.2	
T_{evap}	(°C)	10-35	
T_{cond}	(°C)	20-30	
T_{hot}	(°C)	60-85	
Half cycle	(s)	600-1200	
Heat recovery	(s)	90	

The SDWP for a given cycle time can be estimated by $SDWP_{DA} = N \cdot (q_1 - q_3)$. $SDWP_{DA}$ is based on the DA isotherm and describes the maximum SDWP achievable for a system for a given cycle time. However, the analysis is only applicable to long cycle times > 1000 s, where a real system achieves near equilibrium conditions. Here, $SDWP_{DA}$ approximates the experimental SDWP, while at short and medium cycle times $SDWP_{DA} \gg SDWP$.

The performance indicators depend on the three inlet temperatures to evaporator, condenser and adsorber/desorber. Experimental analyses usually keep two inlet temperatures constant and change the third. However, this complicates the analysis as different results cannot easily be compared. Nuñez et al. addressed this issue by introducing the reduced temperature T_{red} [-], which takes the different temperatures into account in a single parameter [33]:

$$T_{red} = \frac{T_{cond} - T_{evap}}{T_{hot} - T_{cond}} \tag{10}$$

T_{evap}, T_{cond} and T_{hot} are the inlet temperatures [K] to the heat exchangers of the vessels from the cold, ambient and hot thermostatic baths.

The inlet temperatures from the three thermostatic baths have a significant impact on the system performance and there are hundreds of possible combinations. T_{red} is a function of all three inlet temperatures and represents the ratio of the temperature lift to the driving force [33].

T_{red} simplifies the comparison of different inlet temperature since many performance indicators collapse on one single curve if plotted against T_{red}. This occurrence makes T_{red} a useful tool in the prediction of results and the system characterisation.

A single-purpose desalinator is operated at $T_{red} = 0$, where no temperature lift for cooling is desired. Whereas, T_{red} increases depending on the cooling application [34], i.e. in air-conditioning $T_{red} < 0.3$ or in refrigeration $T_{red} > 0.3$.

4. Adsorption cycle analysis

Theoretical analyses of adsorption desalination often focus on the theoretical performance by studying the thermodynamic cycle [26]. This approach neglects the heat and mass transfer limitations of real systems. Fig. 3a complements the theoretical analysis by showing the experimental adsorption cycle at two different cycle times against the thermodynamic cycle, which is assessed through the experimental, average vapour temperatures. The system follows the cycle in a clockwise direction 1→2→3→4→1 in Fig. 3a. The plot can be used to compare the deviation from ideal behaviour and reveals performance limitations at the same time.

In Fig. 3a from 2→3, the pressure inside the condenser is higher than the ideal condensing pressure. This lowers the system performance as the condenser does not operate at ideal conditions. The pressure build-up can be reduced by increasing the condenser surface area [24]. At insufficient condenser area, water vapour desorbs from the material, but cannot condense at the same rate. The limited surface area is not an issue to reach equilibrium, but it increases the cycle time.

The ideal working capacity assessed through the thermodynamic cycle in Fig. 3a is 0.2 kg_w/kg_{sg}. The uptake is reduced to 0.13 kg_w/kg_{sg} at the long half cycle time (1200 s) and at the shorter half cycle time (600 s) to 0.08 kg_w/kg_{sg}.

The shorter cycle time impacts both isosteres and shifts them closer together on both sides in Fig 3a. Thus, at the shorter cycle time neither the adsorption nor desorption capacity of the material are sufficiently used. By contrast, a longer cycle time allows the material to adsorb water sufficiently as the experimental isostere and the thermodynamic isostere 1→2 in Fig. 3a are almost overlapping. The isosteric heating and cooling time was selected based on the time required to increase the pressure to the condenser pressure. The two times of the system are equal to simplify the control sequence.

As a result, the cooling time is slightly longer than necessary, which can be seen from the curve

of the longer cycle time. The pressure inside the adsorber bed goes below the pressure in the evaporator. Once the isosteric cooling time is elapsed, the valve between evaporator and condenser is opened and the pressure inside the adsorber vessel rises to the evaporator pressure. Flash evaporation takes place in the evaporator and the pressure immediately increases (Fig. 3a. The slightly increased isosteric cooling time does not have a negative impact on the performance since the isosteric cooling time is only a fraction of the total cycle time. In addition, the flash evaporation compensates for it.

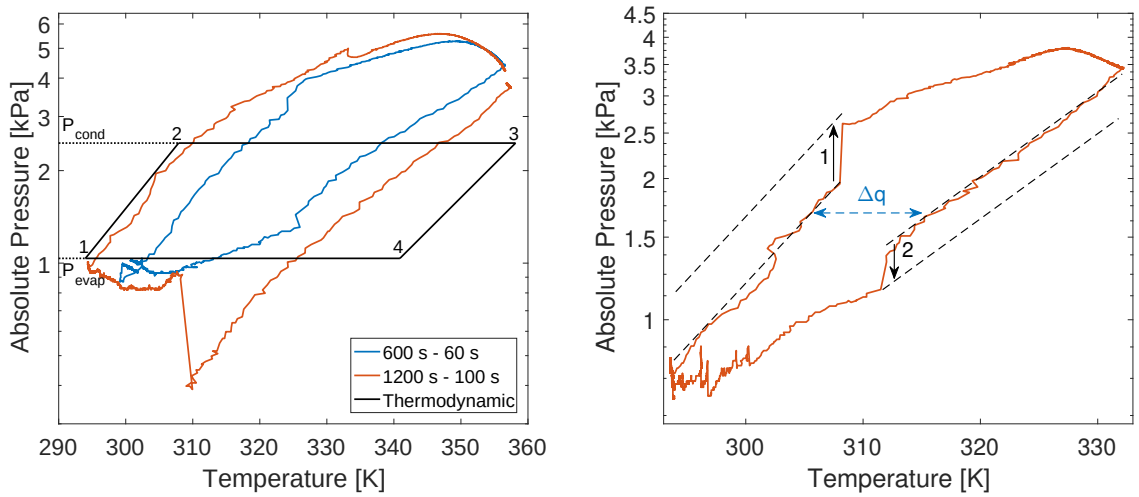

(a) (b)

Figure 3: (a) The influence of the cycle time on the adsorption cycle in comparison to the thermodynamic adsorption cycle in a cooling application. $T_{hot,in}$ = 85 °C, $T_{cond,in}$ = 20 °C and $T_{evap,in}$ = 10 °C. The thermodynamic cycle is based on the average, experimental evaporator and condenser vapour temperatures $T_{evap,vap,av}$ = 7.5 °C and $T_{cond,vap,av}$ = 20.8 °C.
(b) Pressure and temperature changes of the adsorber vessel during one adsorption cycle showing the effect of an insufficient cooling time on the adsorption cycle, which lowers the performance of the system. $T_{hot,in}$ = 60 °C, $T_{cond,in}$ = 20 °C and $T_{evap,in}$ = 10 °C with $t_{ads/des}$=1200 s and t_{isos} = 60 s.

Fig. 3b illustrates how insufficient isosteric heating and cooling times affect the adsorption cycle. During isosteric heating the pressure of the adsorber vessels is still below the condenser pressure. When the valve between the two is opened, a flash evaporation occurs again with water evaporating from the condenser and adsorbing onto the adsorption material. This can be seen in Fig. 3b as the material shifts to a more saturated isostere.

The same effect occurs during isosteric cooling. The valve is opened before the adsorber vessel reaches the lower evaporator pressure and water desorbs from the material into the evaporator, while the material shifts to a drier isostere on the right. Therefore, the material desorbs while it should adsorb. The isosteres in Fig. 3b move further apart from one another, but the useful working capacity Δq remains the same. Thus, more energy is needed to reverse the additional

and adversely occurring adsorption/desorption, which reduces the performance of the system. Therefore, it is imperative to operate at optimal isosteric heating and cooling time to reach $P_{ads} \geq P_{cond}$ before connecting adsorber to condenser during desorption.

Fig. 4 shows the experimental adsorption cycles for five different half cycle times and compares them to the thermodynamic cycle in a desalination application as $T_{cond,in} = T_{evap,in} = 30$ °C. Again, the thermodynamic cycle is assessed through the experimental, average vapour temperatures $T_{evap,vap,av} = 23.5$ °C and $T_{cond,vap,av} = 31.9$ °C of all experiments in Fig. 4. Improved heat transfer of the evaporator heat exchanger would raise $P_{evap}(T_{evap,vap})$ closer towards P_{cond} increasing the working capacity of the material.

The slopes of the experimental isosteres are flatter than the thermodynamic slopes from 1→2 and 3→4 indicating that desorption occurred during these experiments. The adsorber beds are disconnected from evaporator and condenser during the heating and cooling periods. Hence, the flat slopes advert to possible condensation on the adsorber vessel walls during heating 1→2. The condensed water from the vessel walls is adsorbed again during the cooling phase 3→4.

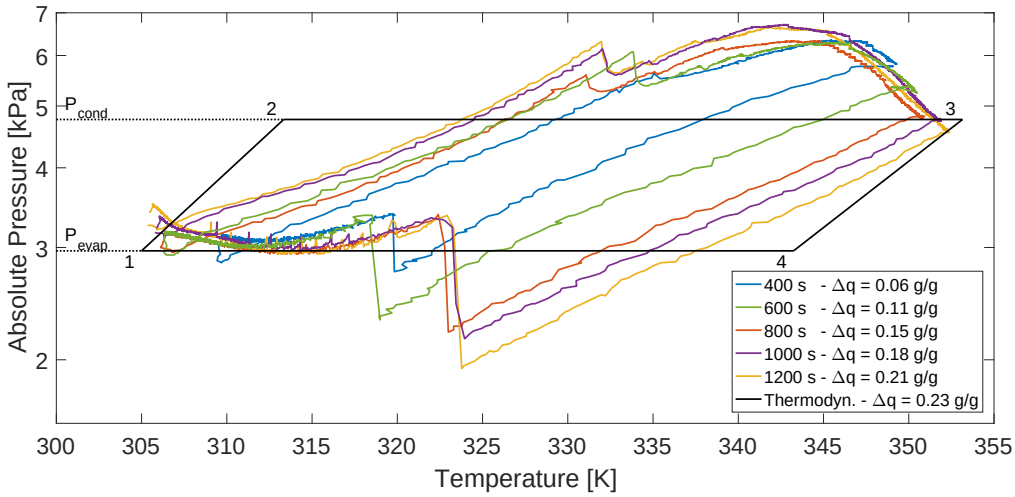

Figure 4: The influence of the cycle time on the adsorption cycle in comparison to the thermodynamic adsorption cycle in a desalination application. $T_{hot,in} = 80$ °C, $T_{cond,in} = T_{evap,in} = 30$ °C and 90 s isosteric heating time. The thermodynamic cycle is based on the average, experimental evaporator and condenser vapour temperatures $T_{evap,vap,av} = 23.5$ °C and $T_{cond,vap,av} = 31.9$ °C.

The cycles in Fig. 4 show that the system reached almost equilibrium at 1200 s half cycle time, because points 1 and 3 are reached at the end of the adsorption and desorption phase. The experimental working capacity at 1200 s is $\Delta q_{exp} = 0.21$ g_w/g_{sg}, which is 0.02 g_w/g_{sg} lower than $\Delta q = 0.23$ g_w/g_{sg} from the thermodynamic analysis. Moreover, cycle times longer than 1200 s would be detrimental to the performance as the system is already close to equilibrium.

At 400 s half cycle time, the working capacity is reduced to 0.06 g_w/g_{sg} (narrow cycle in Fig. 4). Based on the considerations of Fig. 3b, it can be seen that the cooling/heating time of 90 s was sufficient in all experiments of Fig. 4, because the adsorber pressure is above the condenser pressure before the two vessels are connected. The same applies to the desorption phase were the adsorber pressure is below the evaporator pressure causing flash evaporation once the two vessels are connected to each other in point 4.

5. Performance analysis desalination and cooling

The performance of the system varies depending on the cycle time and the temperature of the heating and cooling water supplied to the vessels. Both, the SDWP and SCC collapse on a single curve respectively when plotted over T_{red}. The reduced temperature is a dimensionless quantity, which takes the three system temperatures into account in Eq. (10) allowing the comparison of different temperature lifts and heat source temperatures in a single graph.

In Fig. 5, T_{red} is based on the inlet temperatures to the heat exchangers of the vessels. This allows the comparison of this study to the best performing reference system in the literature presented by Ng et al., because their results are based on the inlet temperatures as well [35, 36]. Desalination applications require $T_{red} < 0.2$, where the two systems show an almost identical performance in Fig. 5. The SDWP is highest at $T_{red} < 0.2$ in Fig 5a as the working capacity increases the closer the pressures in evaporator and condenser are to each other (for low T_{red} in Fig. 2b).

The SCC of the reference system is even exceeded at $T_{red} = 0$. For cooling applications $T_{red} < 0.2$, the performance achieved in this study is below the reference system, which is due to limitations of the evaporator. The performance can be improved by a larger evaporator heat exchanger surface area and spray nozzles, which increase the water surface area and the evaporation rate as in the reference system [36]. Both measures improve the relative humidity (RH) in the evaporator during adsorption, which is the ratio of the vapour pressure in the evaporator and the saturation pressure at the adsorption bed temperature: $RH_{ads} = P_{evap}/P_{sat}(T_{sg})$. The relative humidity for cooling applications is $RH_{ads} < 50$ %, while in desalination it is up to 99 %. The evaporator vapour temperature $T_{evap,vap}$ is as much as 10 °C below $T_{evap,in}$, because of the cooling effect of the evaporating water, which reduces the relative humidity, the evaporation rate and the adsorption uptake.

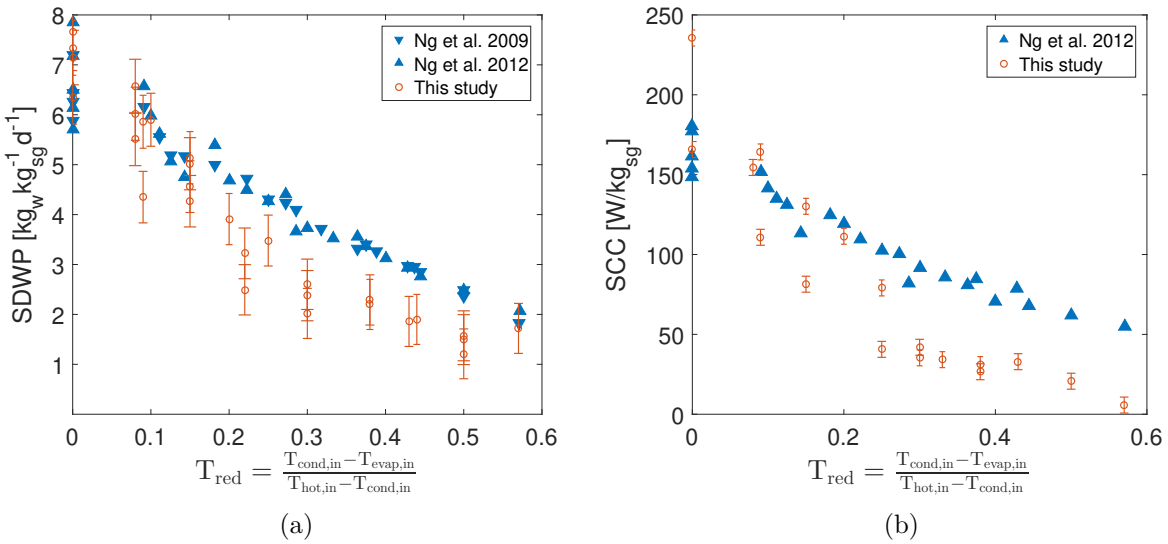

Figure 5: (a) The SDWP plotted over T_{red} based on inlet temperatures in comparison to the literature [35, 36]. The half cycle times are 600 and 1200 s, while $T_{hot,in}$ = 60-85 °C.
(b) The specific cooling capacity plotted over T_{red} in relation to the literature [36]. The half cycle times are 600 and 1200 s while $T_{hot,in}$ = 60-85 °C.

The experiments in Fig. 5 show that at $T_{evap,in} \approx T_{cond,in}$ the vapour temperature in the evaporator is below the condenser vapour temperature $T_{evap,vap} < T_{cond,vap}$, which reduces the relative humidity, working capacity, and performance. For a maximum working capacity and performance, the vapour temperatures need to be equal $T_{evap,vap} \approx T_{cond,vap}$ for $P_{evap} \approx P_{cond}$ as shown in Fig. 2b. Therefore, in Fig. 6a the inlet temperature supplied to the evaporator $T_{evap,in}$ was slightly increased over ambient temperature to improve the system performance. This measure compensates for the cooling effect caused by the evaporating water vapour and leads to $T_{evap,vap} \approx T_{evap,vap}$ for a maximum performance. In Fig. 6a, the reduced temperature is based on the vapour temperatures $T_{red,vap}$ to account for this. The results show that the SDWP increases by 41 % from 7.7 to 10.9 $kg_w/(kg_{sg}d)$ when the system is operated at $T_{evap,vap} \approx T_{cond,vap}$ (Fig. 6a). The result was achieved with the inlet temperatures $T_{hot,in}$ = 80 °C, $T_{cond,in}$ = 25 °C, $T_{evap,in}$ = 35 °C and a half cycle time of 1200 s.

The optimised operational strategy found in this study increases the performance of the adsorption material by maximising the working capacity. Thu et al. used a similar strategy to achieve an SDWP of 9.96 $kg_w/(kg_{sg}d)$ at T_{hot} = 70 °C by implementing an internal heat recovery between evaporator and condenser to their 4-bed adsorption desalinator [27]. The latent heat of the condensing water increases the cooling water outlet temperature, which is then sent to the evaporator to achieve $T_{evap,in} > T_{cond,in}$ leading towards $P_{evap} \approx P_{cond}$.

The system presented in this study is a heat transformer for combined desalination and cool-

ing, whereas Thu et al. presented a system with desalination as single-purpose [27]. In a multi-purpose system, evaporator and condenser cannot be thermally integrated, because the evaporator needs to operate at much lower temperatures than the condenser. In addition, cooling power needs to be extracted from the system, which is not possible with heat integration between the two vessels. Condenser and silica gel release heat during adsorption and this heat is at temperature levels that can hardly power other processes.

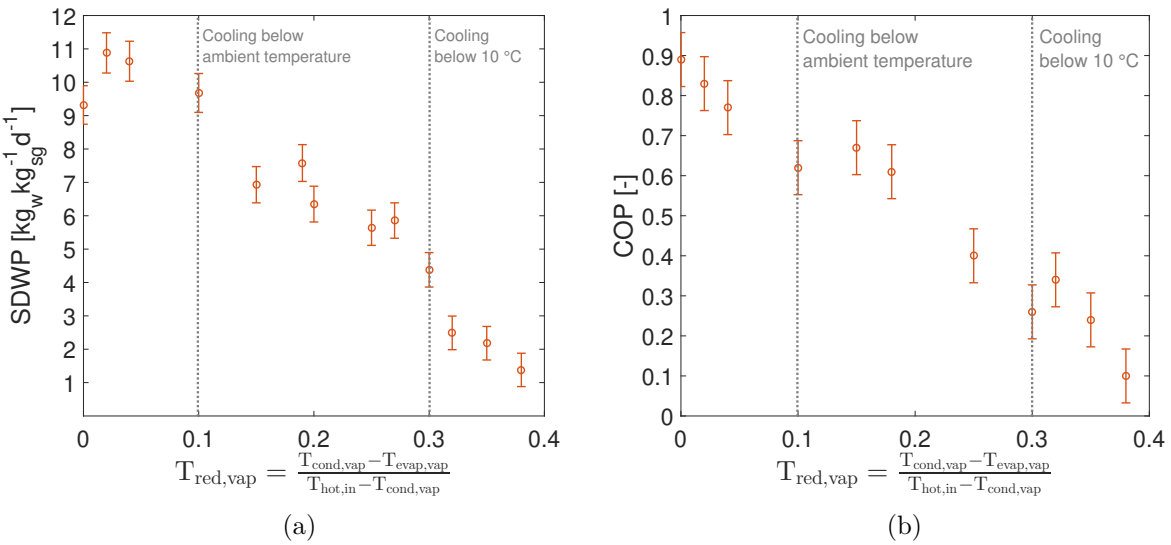

Figure 6: (a) The SDWP investigation extended to cases where $T_{evap,vap} \approx T_{cond,vap}$. Thus, $T_{red,vap}$ is based on the vapour temperatures here. The half cycle times are 600 and 1200 s. 85 °C ≥ $T_{hot,in}$ ≥ 60 °C.
(b) The COP for different $T_{red,vap}$. The half cycle times are 600 - 1200 s including 90 s heat recovery time, ambient temperature 25-30 °C, and T_{hot} ≤ 85 °C.

The combination of chilling and desalination has recently gained a lot of attention [35–40]. Most studies employ silica gel-water as working pair, which is has a good performance for desalination as shown in Fig. 6a at $T_{red} < 0.1$. A change of $T_{red} > 0.1$ in Fig. 6 provides cooling in addition to potable water. However, cooling as well as the water production decrease at higher T_{red}. The system performance is reduced by more than 60 %, when the evaporator is operated below 10 °C, where the COP is reduced from 0.9 to less than 0.3 (Fig. 6b) and SDWP from 10.9 $kg_w/(kg_{sg}d)$ to less than 4.5 $kg_w/(kg_{sg}d)$ (Fig. 6a). Fig. 7 shows that the reduction of the cooling power of the evaporator from 20-80 W at 15 °C to 20-40 W at 10 °C cooling temperature. The results highlight the reduced performance of the silica gel at low evaporator temperatures. Some recent studies proposed different materials for the combined desalination and cooling application.

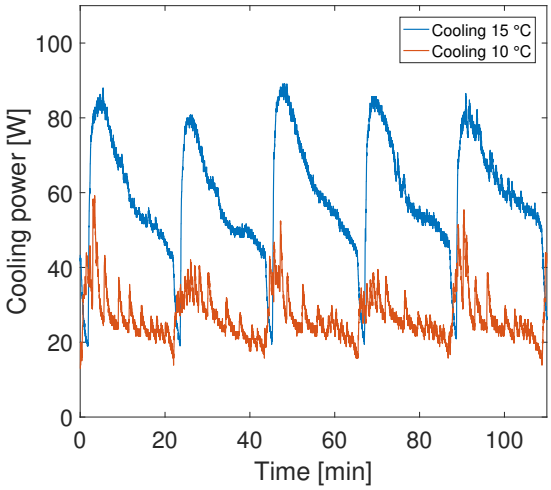

Figure 7: The cooling power decreases significantly with the cooling temperature. T_{hot} = 80 °C, T_{cond} = 20 °C, 1200 s half cycle time and no heat recovery.

Ali et al. proposed the use of copper sulphate as adsorption material for improved cooling and desalination performances. They reported SDWP ≈ 8 $kg_w/(kg_{sg}d)$ and COP ≈ 0.55 for 12 °C at $T_{hot,in}$ = 80 °C, $T_{cond,in}$ = 25 °C and $T_{evap,out}$ = 12 °C [41]. The silica gel system of this study reached SDWP = 6.0 and COP = 0.39 for the same temperatures, which is only 25-30 % below the novel copper sulfate material [41].

Youssef et al. simulated the performance of zeolite AQSOA FAM Z02 with water showing that the material has no performance decrease at low evaporator temperatures, which is an advantage over silica gel, but the performance remains relatively low SDWP ≈ 6-7 $kg_w/(kg_{ad}d)$ [42]. AQSOA FAM Z02 is based on the SAPO-34 zeotype with a chabazite structure [43]. S-shape isotherms as shown by AQSOA FAM Z02 [44] enable constant working capacities over a wide range of evaporator temperatures providing a high cooling power and distillate output at low temperatures [42]. By contrast, silica gel features isotherms that increases asymptotically towards the maximum uptake capacity between 0.3 - 0.4 g_w/g_{sg}. Thus, silica gel adsorbs most water at high evaporator temperatures and high relative humidity limiting the performance in cooling applications [45]. The maximum water uptake of AQSOA FAM Z02 is 0.33 g_w/g_{ad} [46], which is similar to silica gel. Hence, AQSOA FAM Z02 cannot exceed the performance of silica gel in most cases and requires regeneration temperature of at least 80 °C [42]. Elsayed et al.'s work on Metal Organic Frameworks indicated that regeneration temperatures 90-150 °C are necessary to regenerate their material [47]. In addition, the MOF materials show similar behaviour as silica gel with SDWP ≤ 2 $kg_w/(kg_{ad}d)$ at $T_{evap,out}$ = 5 °C and $T_{hot,in}$ ≤ 100 °C. Therefore, the novel materials provide only a marginal improvement compared to silica gel.

A different approach was adapted by Thu et al, who presented a theoretical analysis for a silica gel system featuring two evaporators: one at low temperatures (7-9 °C) and a second evaporator at ambient temperature [48]. During the first part of the half cycel, the silica gel adsorbs water from the low temperature evaporator providing cooling. Adsorption continues from the ambient temperature evaporator until the silica gel is saturated with water. The model predicts a COP below 0.2 for the low temperature evaporator and SDWP $\approx$ 6 $kg_w/(kg_{sg}d)$ for the overall system [48]. Thus, the SDWP and COP of this system configuration are more than twice as high as the results achieved in this study for the same temperatures, but they remain low compared to the performance achieved at high evaporator temperatures $T_{red} > 0.1$. The two evaporator system leads to a performance improvement, but also to a more complex process, which is why more work needs to be done to improve the adsorption material as well as the process, i.e. heat and mass transfer [49, 50].

Novel adsorption materials should feature a high working capacity described by the adsorption isotherms, where S-shaped isotherms are favourable for desalination and cooling applications. Type III isotherms can be beneficial for desalination without cooling, because their uptake exponentially increases at high relative humidity [49]. Heat and mass transfer can either be increased by advanced system design and components [51, 52].

6. Conclusion

In this work, a small-scale adsorption desalinator is used in a comprehensive, experimental adsorption cycle analysis to provide insight into the process beyond the common performance analysis. The adsorption cycle analysis assessed the impact of the system parameters on the adsorption bed and compared the experimental results to the ideal adsorption cycle derived from the Dubinin Astakhov isotherms. The analysis visualised how insufficient heating times reduce the working capacity along with the performance of the system.

The performance of the system was assessed for different inlet temperature combinations, where the inlet temperature to the evaporator was equal or lower than the condenser inlet temperature. The highest Specific Daily Water Production achieved in this series of experiments was 7.7 $kg_w/(kg_{sg}d)$ at $T_{hot,in}$ = 80 °C with a performance ratio of 0.60. However, the results showed that the relative humidity did not exceed 50-60 % during adsorption for these experiments. Hence, slight heating of the evaporator was applied to increase the relative humidity towards 90 %. This measure increased the performance by 41 % to 10.9 $kg_w/(kg_{sg}d)$ at $T_{hot,in}$ = 80 °C,

while it reduced the performance ratio to 0.35 due to the evaporator heating. The results show that the combination of desalination and chilling leads to a performance decrease of 60 %. Therefore, silica gel is not the ideal material for the combined process, but it is a well performing, low-cost material for desalination applications.

Acknowledgements

This work was supported by the RED-Heat-to-Power project (Conversion of Low Grade Heat to Power through closed loop Reverse Electro-Dialysis) - Horizon 2020 programme, Project Number: 640667: `www.red-heat-to-power.eu`

Nomenclature

General

α	Thermal expansion coefficient (1/K)
Δh	Heat of desorption (kJ/kg$_{\mathrm{w}}$)
δ	Modelling parameter (-)
γ_i	Modelling parameter (-)
c_p	Specific heat (kJ/(kg K))
d	Day (d)
E	Dubinin-Astakhov parameter (kJ/kg)
L	Latent heat (kJ/kg)
M_{SG}	Mass of silica gel (kg)
m_w	Mass of water produced (kg)
n	Dubinin-Astakhov parameter (-)
P	pressure (kPa)
Q	Energy (kJ)
q	Water vapour uptake on the silica gel (kg/kg)
q_0	Saturation uptake (kg/kg)
R	Real gas constant (J/(mol K))
T	Temperature (K)
t	Time (s)
t_{cycle}	Cycle time (s)
T_{red}	Reduced temperature (-)
V	Valve
$\dot{m}$	Water flow rate supplied to heat exchanger (kg/s)

Subscripts

ad	Adsorption material
ads	Adsorber
av	Average
$cond$	Condenser
des	Desorption
$evap$	Evaporator
hot	Hot water from heat source
hr	heat recovery
in	Inlet
$isos$	Isosteric
out	Outlet
SAT	Saturation conditions
sg	Silica gel
vap	Vapour

Acronyms

COP	Coefficient of performance (-)
DA	Dubinin Astakhov
MOF	Metal organic framework
PR	Performance ratio (-)
SCC	Specific cooling capacity (W/kg$_{\mathrm{ad}}$)
$SDWP$	Specific Daily Water Production (kg$_{\mathrm{w}}$/(kg$_{\mathrm{sg}}$ d))
$V1$	Valve 1
$V3$	Valve 3

[1] Nels Johnson, Carmen Revenga, and Jaime Echeverria. Managing water for people and nature. *Science*, 292(5519):1071–1072, 2001.

[2] Jan Eliasson. The rising pressure of global water shortages. *Nature*, 517(7532):6–7, 2015.

[3] Kellyn Betts. Technology solutions: Desalination, desalination everywhere. *Environmental Science & Technology*, 38(13):246A–247A, 2004. PMID: 15296291.

[4] A. Tamburini, M. Tedesco, A. Cipollina, G. Micale, M. Ciofalo, M. Papapetrou, W. Van Baak, and A. Piacentino. Reverse electrodialysis heat engine for sustainable power production. *Applied Energy*, 206:1334 – 1353, 2017.

[5] C. Olkis, G. Santori, and S. Brandani. An adsorption reverse electrodialysis system for the generation of electricity from low-grade heat. *Applied Energy*, 231:222 – 234, 2018.

[6] F. Giacalone, C. Olkis, G. Santori, A. Cipollina, S. Brandani, and G. Micale. Novel solutions for closed-loop reverse electrodialysis: thermodynamic characterisation and perspective analysis. *Energy*, 2018.

[7] M. Bevacqua, A. Tamburini, M. Papapetrou, A. Cipollina, G. Micale, and A. Piacentino. Reverse electrodialysis with nh4hco3-water systems for heat-to-power conversion. *Energy*, 137:1293 – 1307, 2017.

[8] Xiang Zheng, Di Chen, Qi Wang, and Zhenxing Zhang. Seawater desalination in china: Retrospect and prospect. *Chemical Engineering Journal*, 242:404 – 413, 2014.

[9] Hisham T El-Dessouky, Hisham M Ettouney, and Yousef Al-Roumi. Multi-stage flash desalination: present and future outlook. *Chemical Engineering Journal*, 73(2):173 – 190, 1999.

[10] Patricia Palenzuela, Ashraf S. Hassan, Guillermo Zaragoza, and Diego-C. Alarcón-Padilla. Steady state model for multi-effect distillation case study: Plataforma solar de almería med pilot plant. *Desalination*, 337:31 – 42, 2014.

[11] Ali Al-Karaghouli and Lawrence L. Kazmerski. Energy consumption and water production cost of conventional and renewable-energy-powered desalination processes. *Renewable and Sustainable Energy Reviews*, 24(Supplement C):343 – 356, 2013.

[12] G. Zaragoza, A. Ruiz-Aguirre, and E. Guillén-Burrieza. Efficiency in the use of solar thermal energy of small membrane desalination systems for decentralized water production. *Applied Energy*, 130:491 – 499, 2014.

[13] Jean-Pierre Mericq, Stéphanie Laborie, and Corinne Cabassud. Evaluation of systems coupling vacuum membrane distillation and solar energy for seawater desalination. *Chemical Engineering Journal*, 166(2):596 – 606, 2011.

[14] Alexander S. Rattner and Srinivas Garimella. Energy harvesting, reuse and upgrade to reduce primary energy usage in the usa. *Energy*, 36(10):6172 – 6183, 2011.

[15] Kim Choon Ng, Kyaw Thu, Youngdeuk Kim, Anutosh Chakraborty, and Gary Amy. Adsorption desalination: An emerging low-cost thermal desalination method. *Desalination*, 308:161 – 179, 2013. New Directions in Desalination.

[16] Sourav Mitra, Pramod Kumar, Kandadai Srinivasan, and Pradip Dutta. Performance evaluation of a two-stage silica gel + water adsorption based cooling-cum-desalination system. *International Journal of Refrigeration*, 58:186 – 198, 2015.

[17] Ahmed S. Alsaman, Ahmed A. Askalany, K. Harby, and Mahmoud S. Ahmed. Performance evaluation of a solar-driven adsorption desalination-cooling system. *Energy*, 128:196 – 207, 2017.

[18] Paulo J. Vodianitskaia, José J. Soares, Herbert Melo, and José Maurício Gurgel. Experimental chiller with silica gel: Adsorption kinetics analysis and performance evaluation. *Energy Conversion and Management*, 132:172 – 179, 2017.

[19] Alessio Sapienza, Giuseppe Gullì, Luigi Calabrese, Valeria Palomba, Andrea Frazzica, Vincenza Brancato, Davide La Rosa, Salvatore Vasta, Angelo Freni, Lucio Bonaccorsi, and Gaetano Cacciola. An innovative adsorptive chiller prototype based on 3 hybrid coated/granular adsorbers. *Applied Energy*, 179:929 – 938, 2016.

[20] Maciej Chorowski and Piotr Pyrka. Modelling and experimental investigation of an adsorption chiller using low-temperature heat from cogeneration. *Energy*, 92:221 – 229, 2015. Special Issue devoted to the Polish Energy Mix Conference.

[21] V.E. Sharonov and Yu.I. Aristov. Chemical and adsorption heat pumps: Comments on the second law efficiency. *Chemical Engineering Journal*, 136(2):419 – 424, 2008.

[22] Mohammad A. Al-Ghouti, Ibrahim Yousef, Rafat Ahmad, Ayoup M. Ghrair, and Ayman A. Al-Maaitah. Characterization of diethyl ether adsorption on activated carbon using a novel adsorption refrigerator. *Chemical Engineering Journal*, 162(1):234 – 241, 2010.

[23] Q.W. Pan, R.Z. Wang, L.W. Wang, and D. Liu. Design and experimental study of a silica gel-water adsorption chiller with modular adsorbers. *International Journal of Refrigeration*, 67:336 – 344, 2016.

[24] Nejib Douss, Francis E Meunier, and Lian Ming Sun. Predictive model and experimental

results for a two-adsorber solid adsorption heat pump. *Industrial & engineering chemistry research*, 27(2):310–316, 1988.

[25] H.T. Chua, K.C. Ng, A. Malek, T. Kashiwagi, A. Akisawa, and B.B. Saha. Modeling the performance of two-bed, sillica gel-water adsorption chillers. *International Journal of Refrigeration*, 22(3):194 – 204, 1999.

[26] Jun W. Wu, Eric J. Hu, and Mark J. Biggs. Thermodynamic cycles of adsorption desalination system. *Applied Energy*, 90(1):316 – 322, 2012. Energy Solutions for a Sustainable World, Special Issue of International Conference of Applied Energy, ICA2010, April 21-23, 2010, Singapore.

[27] Kyaw Thu, Hideharu Yanagi, Bidyut Baran Saha, and Kim Choon Ng. Performance investigation on a 4-bed adsorption desalination cycle with internal heat recovery scheme. *Desalination*, 402:88 – 96, 2017.

[28] Douglas M Ruthven. *Principles of adsorption and adsorption processes*. John Wiley & Sons, 1984.

[29] C. Olkis, S. Brandani, and G. Santori. A small-scale adsorption desalinator. *Energy Procedia*, 158:1425 – 1430, 2019. Innovative Solutions for Energy Transitions.

[30] Alessio Sapienza, Andreas Velte, Ilya Girnik, Andrea Frazzica, Gerrit Füldner, Lena Schnabel, and Yuri Aristov. "water - silica siogel" working pair for adsorption chillers: Adsorption equilibrium and dynamics. *Renewable Energy*, 110(Supplement C):40 – 46, 2017.

[31] M. M. Dubinin and V. A. Astakhov. Development of the concepts of volume filling of micropores in the adsorption of gases and vapors by microporous adsorbents. *Bulletin of the Academy of Sciences of the USSR, Division of chemical science*, 20(1):3–7, Jan 1971.

[32] Giulio Santori and Chiara Di Santis. Optimal fluids for adsorptive cooling and heating. *Sustainable Materials and Technologies*, 12:52 – 61, 2017.

[33] Tomas Núñez, Walter Mittelbach, and Hans-Martin Henning. Development of an adsorption chiller and heat pump for domestic heating and air-conditioning applications. *Applied Thermal Engineering*, 27(13):2205 – 2212, 2007. Heat Powered Cycles – 04.

[34] Yu.I. Aristov, D.M. Chalaev, B. Dawoud, L.I. Heifets, O.S. Popel, and G. Restuccia. Simulation and design of a solar driven thermochemical refrigerator using new chemisorbents.

Chemical Engineering Journal, 134(1):58 – 65, 2007. Proceedings of the XVII International Conference on Chemical Reactors CHEMREACTOR-17 and Post-Symposium "Catalytic Processing of Renewable Sources: Fuel, Energy, Chemicals".

[35] Kim Choon Ng, Kyaw Thu, Anutosh Chakraborty, Bidyut Baran Saha, and Won Gee Chun. Solar-assisted dual-effect adsorption cycle for the production of cooling effect and potable water. *International Journal of Low-Carbon Technologies*, 4(2):61–67, 2009.

[36] Kim Choon Ng, Kyaw Thu, Bidyut Baran Saha, and Anutosh Chakraborty. Study on a waste heat-driven adsorption cooling cum desalination cycle. *International Journal of Refrigeration*, 35(3):685 – 693, 2012. Refrigeration and Heat Pumping with Sorption Processes.

[37] Peter G. Youssef, Saad M. Mahmoud, and Raya K. AL-Dadah. Numerical simulation of combined adsorption desalination and cooling cycles with integrated evaporator/condenser. *Desalination*, 392:14 – 24, 2016.

[38] Peter G. Youssef, Hassan Dakkama, Saad M. Mahmoud, and Raya K. AL-Dadah. Experimental investigation of adsorption water desalination/cooling system using cpo-27ni mof. *Desalination*, 404(Supplement C):192 – 199, 2017.

[39] Sourav Mitra, Kyaw Thu, Bidyut Baran Saha, Kandadai Srinivasan, and Pradip Dutta. Modeling study of two-stage, multi-bed air cooled silica gel+water adsorption cooling cum desalination system. *Applied Thermal Engineering*, 114:704 – 712, 2017.

[40] Bidyut Baran Saha, Ibrahim I. El-Sharkawy, Muhammad Wakil Shahzad, Kyaw Thu, Li Ang, and Kim Choon Ng. Fundamental and application aspects of adsorption cooling and desalination. *Applied Thermal Engineering*, 97:68 – 76, 2016. Polygeneration processes, systems, technologies and applications.

[41] Ehab S. Ali, Ahmed A. Askalany, K. Harby, Mohamed Refaat Diab, and Ahmed S. Alsaman. Adsorption desalination-cooling system employing copper sulfate driven by low grade heat sources. *Applied Thermal Engineering*, 136:169 – 176, 2018.

[42] Peter G. Youssef, Saad M. Mahmoud, and Raya K. AL-Dadah. Performance analysis of four bed adsorption water desalination/refrigeration system, comparison of aqsoa-z02 to silica-gel. *Desalination*, 375:100 – 107, 2015.

[43] Charithea Charalambous, Giulio Santori, Enrique Vilarrasa-Garcia, Moises Bastos-Neto, Célio L Cavalcante Jr, and Stefano Brandani. Pure and binary adsorption of carbon dioxide and nitrogen on aqsoa fam z02. *Journal of Chemical & Engineering Data*, 63(3):661–670, 2018.

[44] Stefan K Henninger, Sebastian-Johannes Ernst, Larisa Gordeeva, Phillip Bendix, Dominik Fröhlich, Alexandra D Grekova, Lucio Bonaccorsi, Yuri Aristov, and Jochen Jaenchen. New materials for adsorption heat transformation and storage. *Renewable Energy*, 110:59 – 68, 2017. Increasing the renewable share for heating and cooling by the means of sorption heat pumps and chillers.

[45] S.K. Henninger, F.P. Schmidt, and H.-M. Henning. Water adsorption characteristics of novel materials for heat transformation applications. *Applied Thermal Engineering*, 30(13):1692 – 1702, 2010.

[46] Vincenza Brancato and Andrea Frazzica. Characterisation and comparative analysis of zeotype water adsorbents for heat transformation applications. *Solar Energy Materials and Solar Cells*, 180:91 – 102, 2018.

[47] Eman Elsayed, Raya AL-Dadah, Saad Mahmoud, Paul.A. Anderson, Ahmed Elsayed, and Peter G. Youssef. Cpo-27(ni), aluminium fumarate and mil-101(cr) mof materials for adsorption water desalination. *Desalination*, 406:25 – 36, 2017. Desalination and the Environment.

[48] Kyaw Thu, Bidyut Baran Saha, Kian Jon Chua, and Kim Choon Ng. Performance investigation of a waste heat-driven 3-bed 2-evaporator adsorption cycle for cooling and desalination. *International Journal of Heat and Mass Transfer*, 101:1111 – 1122, 2016.

[49] Ahmed A. Askalany, Angelo Freni, and Giulio Santori. Supported ionic liquid water sorbent for high throughput desalination and drying. *Desalination*, 452:258 – 264, 2019.

[50] Animesh Pal, Maisara Shahrom Raja Shahrom, Muhammad Moniruzzaman, Cecilia Devi Wilfred, Sourav Mitra, Kyaw Thu, and Bidyut Baran Saha. Ionic liquid as a new binder for activated carbon based consolidated composite adsorbents. *Chemical Engineering Journal*, 326:980 – 986, 2017.

[51] X. Zheng, R.Z. Wang, T.S. Ge, and L.M. Hu. Performance study of sapo-34 and fapo-34 desiccants for desiccant coated heat exchanger systems. *Energy*, 93:88 – 94, 2015.

[52] L. Calabrese, V. Brancato, L. Bonaccorsi, A. Frazzica, A. Caprì, A. Freni, and E. Proverbio. Development and characterization of silane-zeolite adsorbent coatings for adsorption heat pump applications. *Applied Thermal Engineering*, 116:364 – 371, 2017.